Asian Journal of Chemistry; Vol. 37, No. 12 (2025), 3065-3072
ASIAN JOURNAL OF CHEMISTRY
https://doi.org/10.14233/ajchem.2025.34681

Green Synthesis and *in vitro* Antioxidant and Anticancer Activities of Copper Nanoparticles from *Asparagus racemosus* Chloroform Extract

JITENDRA DEBATA[1], DHIRAJ KUMAR[2], SUJIT KUMAR SAHU[3], TANDRIMA MAJUMDER[4] and SANDIP SEN[5,*]

[1]Department of Pharmaceutical Chemistry, Bengal College of Pharmaceutical Technology, Dubrajpur, Birbhum-731123, India
[2]Department of Pharmaceutical Analysis, Institute of Technology and Management, GIDA, Gorakhpur-273212, India
[3]Department of Pharmaceutical Chemistry, Institute of Pharmacy & Technology, Salipur, Cuttack-754202, India
[4]Department of Pharmaceutical Chemistry, College of Pharmacy, COER University, Roorkee, Haridwar-247667, India
[5]Department of Pharmaceutical Chemistry, School of Pharmacy, Guru Nanak Institutions Technical Campus, Khanapur, Ibrahimpatnam-501506, India

*Corresponding author: E-mail: sandipsen2010@gmail.com

Received: 11 August 2025 *Accepted*: 9 October 2025 *Published online*: 30 November 2025 AJC-22196

Asparagus racemosus has a wide range of therapeutic activities due to different types of phytoconstituents like glycosides, alkaloids, steroids, tannins, lignins and other bioactive substances. To enhance the therapeutic efficacy of the highly non-polar chemicals present in the chloroform extract, the current study aimed to develop metallic nanoparticles using $CuSO_4 \cdot 5H_2O$ at 1 Mm copper sulphate. The extraction was carried out by Soxhlet apparatus using petroleum ether. The identification of the potential bioactive compound was done by GC-MS analysis. The optimization and characterization of the metallic nanoparticles were done by UV-Spectroscopy, particle size and zeta analysis, ESEM, TEM, FTIR and TGA. The *in vitro* antioxidant and anticancer activity were determined for the optimized formulation, moreover, *in silico* study was done by Swiss ADME, Moleinspiration and Oawasis data warrior software. The completion of the reaction was observed due to a change in absorption maxima. The particle size was determined to be 276.2 ± 8.1 nm, with a zeta potential of -50.09 ± 7.5 mV and a polydispersity index (PDI) of 0.29. The optimized nanoparticles exhibited a spherical morphology with a well-defined concentric bilayer membrane. No chemical incompatibilities were detected for the optimized formulation. Thermogravimetric and differential thermal analyses indicated favourable thermal stability, supporting a good shelf-life profile. The optimized nanoparticles exhibited good therapeutic efficacy due to improvement in the permeability of the chloroform extract and major constituent, steroidal compound pregn-5-ene-3,11-dione, 17,20:20,21-*bis*[methylene*bis*(oxy)]-, cyclic 3-(1,2-ethanediyl acetal).

Keywords: *Asparagus racemosus*, Metallic nanoparticles, Zeta potential, Morphology, Thermal analysis, Antioxidant, Anticancer activity.

INTRODUCTION

In Ayurvedic medicine, Shatavari (*Asparagus racemosus* Willd.), belongs to the family Asparagaceae, known for its multiple therapeutic effects [1]. Shatavari has strong anti-ulcer, anti-inflammatory, immunomodulatory and antioxidant activities. It's also lower stress-induced physiological reactions, have been likened to those of Panax ginseng [2]. It has a good therapeutic index in treating female reproductive disorders such as lactation insufficiency, menopause and premenstrual syndrome [3]. The galactagogue potential of *A. racemosus* was confirmed by a randomized controlled trial [4], which showed that supplementing with the plant increased prolactin levels and breast milk production in postpartum women. The literature also revealed gastric ulcer healing capacity of satavari due to mucilage and antioxidant [5,6]. It is also reported immunomodulatory effect, demonstrating elevated phagocytic activity and lymphocyte proliferation [1]. The increasing interest in using Shatavari in contemporary herbal formulations and functional foods is supported by these complex pharmacological actions [7].

The bioactive molecules derived from the plant extracts loss the potency in gastric environment. To overcome this limitation, metallic nanoparticles (MNPs) have attracted significant attention due to their high surface area, physicochemical stability and gastrointestinal resilience [8,9]. MNPs are particu-

This is an open access journal, and articles are distributed under the terms of the Attribution 4.0 International (CC BY 4.0) License. This license lets others distribute, remix, tweak, and build upon your work, even commercially, as long as they credit the author for the original creation. You must give appropriate credit, provide a link to the license, and indicate if changes were made.

larly well-suited for applications in drug delivery, biomedical imaging and catalysis [10]. Common metallic nanoparticles, such as silver (Ag), gold (Au), copper (Cu) and platinum (Pt), exhibit unique properties. For instance, silver nanoparticles exhibit broad-spectrum antimicrobial activity, while gold nanoparticles are favoured for targeted drug delivery and photothermal therapy due to their biocompatibility and facile surface modification [11].

Green synthesis approaches allow the fabrication of metallic nanoparticles tailored for specific applications by selecting suitable metal salts and plant-derived reducing agents. However, their long-term toxicity and environmental impact necessitate careful evaluation to ensure safe use [12]. Ongoing research focuses on enhancing efficacy and biocompatibility through hybrid systems and functionalized nanoparticles [13]. Among these, copper nanoparticles have emerged as promising candidates due to their antioxidant, antimicrobial and anticancer properties, as well as their sustainability and biocompatibility [14].

The present investigation indicates the presence of potentially bioactive non-polar molecules in the chloroform extract of *A. racemosus*, which will be identified using GC-MS and supported by *in silico* analysis. To enhance the therapeutic efficacy, copper nanoparticles were green-synthesized and characterized with respect to particle size, morphology and stability using zeta potential and thermal analyses. Their biological activity was evaluated through *in vitro* antimicrobial and antioxidant assays.

EXPERIMENTAL

Collection of plant material: At 373 m (1,224 feet) at 16.5811ºN 77.7489ºE, fresh stems of *Asparagus racemosus* were gathered from Ibrahimpatnam, India. The plant materials were authenticated by the Department of Botany, Osmania University, Hyderabad, India.

Preparation of extract: At 40 ± 5 ºC, the fresh plant materials were allowed to air-dry in shade. Crompton TRET500 (made in India) mixer and grinder was used to grind the dry plant material to a coarse powder. The stem powdered was first defatted using petroleum ether (60 ºC fraction). The extraction was then carried out using a Soxhlet apparatus. Approximately 200 g of stem powder, enclosed in a muslin bag of 100-mesh size, was subjected to continuous extraction with chloroform (1 L) until the siphoning solvent became colourless. A rotary flash evaporator (Rotavapor R-300 Buchi, India) with a reduced pressure setting of 55 ºC and 50 rpm was used to collect the petroleum ether layer. The percentage yield was calculated after allowing the extract to dry completely in a desiccator to obtain a constant weight [15].

Phytochemical analysis: The chloroform extract was subjected to phytochemical analysis following established literature procedures [16].

GC-MS analysis: The GC-MS analysis was carried out using an AccuTOF GCv/JMS-T100GCv mass spectrometer coupled to an Agilent 7890A GC system (JEOL). A solution prepared by dissolving 100 mg of chloroform extract in 100 mL of HPLC-grade methanol and diluting it to 30 µg/mL was used for analysis, which was carried out over a 50 min run. An HP-5 column (30 m × 0.25 mm × 0.25 µm) was employed for chromatographic separation, with helium supplied as the carrier gas at 1 mL/min and the oven maintained at 280 ºC; the resulting mass spectra were matched with the NIST database for compound identification [17,18].

Preparation of structure and *in silico* study: The SMILES notation was obtained from ACD Labs Chemsketch version 12.0, The Swiss ADME online tool and Osiris data warrior software were utilized to ascertain the pharmacokinetic, toxicity potential, bioactivity score, physicochemical drug likelihood and molecular characteristics. The therapeutic potential of the identified molecules was assessed using the Swiss Target Prediction platform [19]. The % Abs was determined by using the formula:

$$\text{Absorbance (\%)} = 109 - (0.345 \times \text{TPSA})$$

Synthesis of copper nanoparticles: A chloroform extract (10 mL of 10% w/v) was added to 10 mL of $CuSO_4 \cdot 5H_2O$ solution of different concentrations (Table-1) dropwise. The reaction mixture was stirred magnetically using thermostate magnetic stirrer Remi 5MLH 5 L at 100 rpm. The mixture was heated at 60 ºC for 1 h. The colour was changed from brown to green colour with the progress of reaction. The pH of the solution was maintained at 7.2 to achieve complete precipitation. The resulting mixture was homogenized at 10,000 rpm for 30 min using a Remi RQ-127 A/D homogenizer, followed by centrifugation at 10,000 rpm with a Remi CM-8 Plus cooling centrifuge (4 × 50 mL swing-out rotor). The precipitate was collected, stored in an Amber-coloured container, and used to determine the percentage yield, while the supernatant was reserved for estimation of entrapment efficiency [20].

Determination of absorption maxima: The spectroscopic analysis was determined by Labman spectrophotometer LMS-PUV1920, India. The chloroform extract (50 mg) was dissolved in 50 mL of phosphate buffer (pH 6.8). A portion of this solution was further diluted to 30 µg/mL for analytical measurements. For overlay spectrum preparation, 10 mL of copper(II) nanoparticle solution was diluted to 50 mL [21].

Entrapment efficiency: The ultra-centrifugation technique was used to measure the entrapment efficiency. The freshly prepared copper(II) nanoparticles (2 mL) was centrifuged for 30 min at 10000 rpm (Remi cooling centrifuge, Remi, India). The supernatant (1 mL) was diluted with 9 mL of buffer to a final volume of 10 mL, and its absorbance was measured by UV-visible spectrophotometry to calculate the percentage entrapment efficiency (% EE) [22]. The data was represented in the form of mean ± standard deviations:

TABLE-1
COMPOSITION OF NANOPARTICLES

Component	SCCN1	SCCN2	SCCN3	SCCN4	SCCN5
Extract (%)	10	10	10	10	10
$CuSO_4 \cdot 5H_2O$ (mM)	0.25	0.5	0.75	1	1.25

$$EE\ (\%) = \frac{C_1 - C_2}{C_1} \times 100$$

Size distribution, zeta potential and polydispersity index: The Malvern Zetasizer (Malvern Instruments, Southborough, UK) was employed to analyze the vesicle size, polydispersity index (PDI) and zeta potential of phytosomes [23]. After filling the cuvette with the diluted sample, the analysis was conducted at 25 ± 2 ºC and a scattering angle of 90º. A refractive index of 1.330 and 0.050 absorptions were used for the measurement. An electrode cuvette was used to evaluate the zeta potential of sample. Every study was conducted in triplicate and the mean ± standard deviations were used to represent the data.

Environmental scanning electron microscopy: ESEM analysis was performed using a FEI Quanta 200 (Hillsboro, USA). Two drops of the samples (40 µL) were deposited on the conducting copper tap and air-dried. Each sample received a platinum sputter coating with a thickness of 10 nm and analyzed under the microscope at 10000X magnification scales [23].

Transmission electron microscopy: A TEM device (JEM 2100F, Japan) was utilized to analyze the morphology of optimized nanoparticles. A drop of the sample was placed onto a copper grid coated with 200-mesh carbon, and excess solvent was removed using filter paper. After air-drying, the grid was examined under a TEM, and images were captured using the associated software [23].

FTIR analysis: FTIR analysis was performed using a Bruker 3000 Hyperion Microscope coupled with a Vertex 80 FTIR system (Germany) in Micro ATR grazing angle mode. Approximately 1 mg of extract was placed on the sampling plate and scanned over the range 4000–450 cm^{-1} [24].

Thermal analysis: Thermal analysis was carried out using Hitachi NEXTA STA300 (India). Thermal analysis of 27.429 mg of the sample was performed in a ceramic crucible under nitrogen, with temperature ranged from 30 to 800 ºC at 10 ºC/0.2 s to evaluate thermal stability and weight loss [25].

***In vitro* antioxidant activity (DPPH method):** The solutions of the extract, nanoparticles, and standard were prepared at concentrations of 25, 50, 75, 100 and 125 µg/mL. To each sample, 2 mL of 0.004% DPPH solution was added, and the mixtures were incubated for 30 min at room temperature under light to allow the reaction to proceed. Absorbance was measured at 517 nm using a UV-Visible spectrophotometer. All experiments were performed in triplicate and percentage inhibition and IC_{50} values were calculated [26].

$$\text{Inhibition}\ (\%) = \frac{Abs_{control} - Abs_{test}}{Abs_{control}} \times 100$$

***In vitro* anticancer activity (MTT assay method):** The MTT assay was used to assess the *in vitro* anticancer activity of a plant extract and its nanoparticle formulation against the cell lines MCF-7 (breast cancer) and LNCaP (prostate cancer). The cells were kept at 37 ºC with 5% CO_2 in DMEM supplemented with 10% FBS and 1% penicillin-streptomycin. After the cells reached 80-90% confluency, they were seeded in 96-well plates (5×10^4 cells/well) and given different concentrations of the test samples (25-100 µg/mL) for 24-48 h along with a standard drug, doxorubicin. After treatment, MTT reagent was added to evaluate cell viability. The cells were then dissolved in DMSO and their absorbance at 570 nm was measured. GraphPad Prism 5 were used to calculate the percentages of cell viability and inhibition as well as the IC_{50} values. Every test was carried out in triplicate while maintaining the aseptic conditions [27].

Statistical analysis: Statistical analysis was done using the software Graphpad Prism 5. Each study was done in triplicate and data were represented in the form of mean ± SD or mean ± SEM.

RESULTS AND DISCUSSION

According to the reports, the pharmacological properties of the root extract of *A. racemosus* include immunomodulatory, antidiabetic, antioxidant, antiulcer and antidiarrheal properties. The present study was aimed to improve the therapeutic efficacy of the nonpolar compounds identified in chloroform extract [17]. The extraction yielded 21.31% of the petroleum ether fraction. Phytochemical analysis confirmed the presence of highly non-polar compounds, including terpenoids, steroids, lignin, and alkaloids. GC-MS analysis of the extract (Fig. 1) revealed a total of 11 compounds, with the highest peak area (42.28%) corresponding to compound 8, which exhibited a retention time of 23.44 min. The structure of this compound was further confirmed by mass spectrometry (Fig. 2) and identified as pregn-5-ene-3,11-dione, 17,20:20,21-bis[methylene-bis(oxy)]-, cyclic 3-(1,2-ethanediyl acetal). Based on its structural features, the compound was classified as a steroidal alkaloid [17]. Moreover, this compound has demonstrated its potential antioxidant and antimicrobial activity, with *in silico* studies indicating favourable pharmacokinetic properties, bioactivity scores against enzymes, and promising anticancer activity based on target prediction [17].

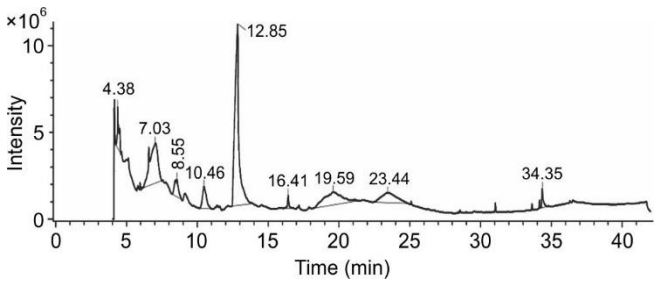

Fig. 1. GC-MS analysis for chloroform extract of *A. racemosus* [Ref. 15]

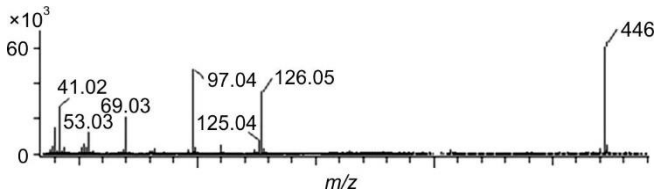

Fig. 2. Mass spectrum for molecule-8 isolated from the chloroform extract of *A. racemosus* [Ref. 15]

***In silico* study and target prediction:** The isolated molecule exhibited good physicochemical properties in respect to distribution coefficient, TPSA, percentage of absorption (Table-2). The major limitation of the compound is its poor

TABLE-2
In silico STUDIES FOR MOLECULE-8 CHLOROFORM EXTRACT OF *Asparagus racemosus* (SHATAVARI) [Ref. 15]

Physico-chemical properties	
cLogP	2.28
cLogS	-4.76
H-acceptors	7
H-donors	0
Molar refractivity	113.32
TPSA	72.45
%Absorption	84.00
Solubility	Insoluble soluble
Molecular property	
Shape index	0.43
Molecular flexibility	0.22
Molecular complexity	1.02
Toxicity potential	
Mutagenic	No
Tumorigenic	No
Reproductive effective	Yes
Irritant	No
Pharmacokinetic properties	
GI absorption	High
BBB permeant	Yes
Pgp substrate	No
CYP1A2 inhibitor	No
CYP2C19 inhibitor	No
CYP2C9 inhibitor	No
CYP2D6 inhibitor	No
CYP3A4 inhibitor	No
log Kp (cm/s)	-7.46
Drug likeliness	
Drug likeness	-5.62
Lipinski	Yes
Veber	Yes
Egan	Yes
Muegge	Yes
Bioavailability score	0.55
Bioactivity score	
GPCR ligand	0.22
Ion channel modulator	0.16
Nuclear receptor ligand	0.12
Protease inhibitor	0.22
Enzyme inhibitor	0.41
Target prediction	
Thymidine kinase enzyme (Kappa opioid receptor)	Anticancer
Family A G protein-coupled receptor	Anticancer

solubility, which is influenced by its spherical structure and low molecular flexibility. Despite this, the molecule exhibited no toxicity, favourable pharmacokinetic properties and acceptable drug-likeness. Its bioavailability was moderate, while bioactivity predictions indicated good GPCR ligand binding affinity and potential anti-inflammatory activity [17]. To overcome the solubility and bioavailability limitations, metallic nanoparticles were developed from the petroleum ether extract.

Optimization of synthesis of metallic nanoparticles: The synthesis of nanoparticles was optimized using a fixed extract concentration (10% w/v) and varying concentrations of copper sulphate (mM). At low concentrations, simple complexation occurred, whereas higher concentrations (0.75 and 1 mM) led to the chelate formation. The resulting chelates were stable at pH 7.2 and homogenized at 10,000 rpm to achieve nanoparticles within the desired size range. The size of the nanoparticles increased with the increase in concentration of salt. However, the concentrations above 1.25 mM resulted in precipitation, indicating a threshold for stable nanoparticle formation. The completion of the reaction was determined by spectroscopic method. There was change in absorption band with the completion of reaction [28]. The absorption maxima for the nanoparticles was found to be 450 nm (Fig. 3).

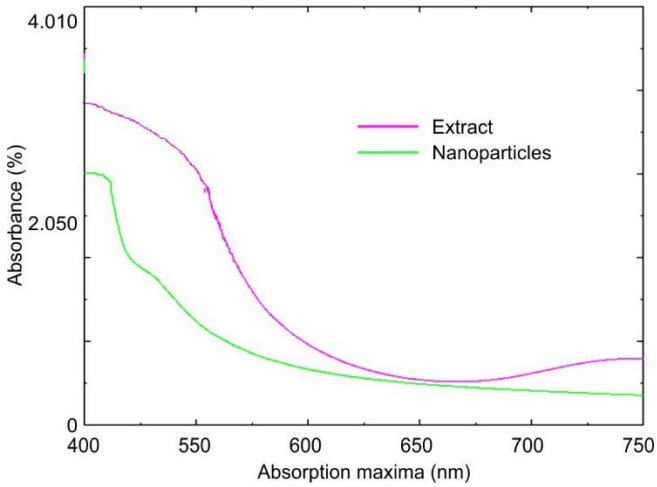

Fig. 3. Absorption maxima of the extract and its copper nanoparticles

Entrapment efficiency (EE%): The entrapment efficiency provides valuable information regarding the entrapment of the extract encapsulated due to metal complexation. The efficacy of the nanoparticles depends on the amount of the extract encapsulated by complexation [29,30]. The entrapment efficiency was found to be 67.00 ± 1.44 to 92.00 ± 2.09. There was formation of chelates at 0.75 and 1 mM and precipitation at 1.25 mM. High metal concentration increases the surface morphology, particle size and release property also due to strong ionic bonding [31]. The physical appearance at 0.75 and 1 mM exhibited % EE of 85.33 ± 1.36 and 92.00 ± 2.09, respectively (Fig. 4).

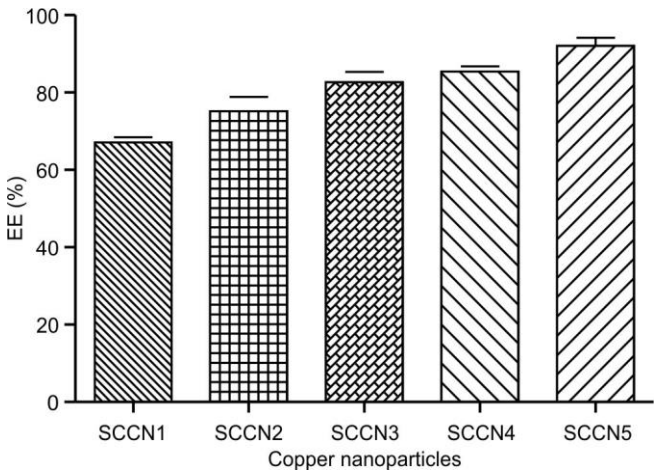

Fig. 4. Entrapment efficiency data of the synthesized nanoparticles

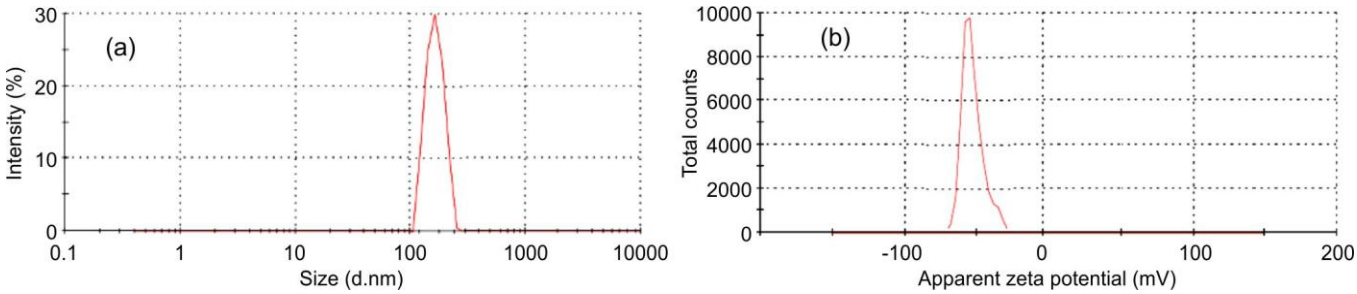

Fig. 5. (a) Particle size and (b) zeta potential plots of the nanoparticles SCCN4

Particle size and zeta potential: The size and zeta potential of the nanoparticles depends on concentration of the metal ions. High concentration of metal ion increases particle size and reduce stability [32]. The particle size was found to be 180.4 ± 4.5 to 297.3 ± 7.3. The zeta potential value was found to be -20.1 ± 3.2 to -50.21 ± 7.5. The PDI value was found to be 0.21 to 0.35 indicate with gradual increase in metallic ion concentration the solution become polydisperse [33]. There was good stability (zeta potential) was observed for the nanoparticles coded with SCCN3 and SCCN4 -41.02 and -50.09 mV (Table-3 and Fig. 5).

TABLE-3
VESICLE SIZE, ZETA POTENTIAL AND POLYDISPERSITY INDEX OF OPTIMIZED NANOPARTICLES

Formulation	Z average (d.nm) ± SD	Zeta potential (mV) ± SD	PdI
SCCN1	180.4 ± 4.5	-20.10 ± 3.2	0.21
SCCN2	201.5 ± 6.4	-28.20 ± 3.4	0.23
SCCN3	232.1 ± 5.2	-41.02 ± 4.1	0.25
SCCN4	276.2 ± 8.1	-50.21 ± 7.5	0.29

All the studies carried out in triplicate and datas are represented in Mean ± SD.

SEM and TEM analysis: SEM analysis was conducted on the CNp4 nanoparticles, revealing a predominantly spherical morphology, which is favourable for enhanced drug absorption [34]. This spherical structure observed in SEM (Fig. 6) was further confirmed by TEM imaging (Fig. 7), which additionally demonstrated a concentric bilayer membrane, indicating well-defined and stable nanoparticle architecture.

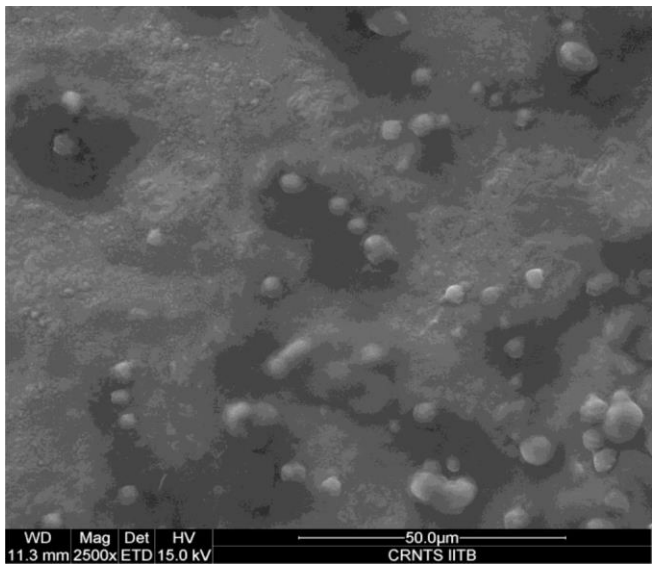

Fig. 6. SEM image of the nanoparticles SCCN4

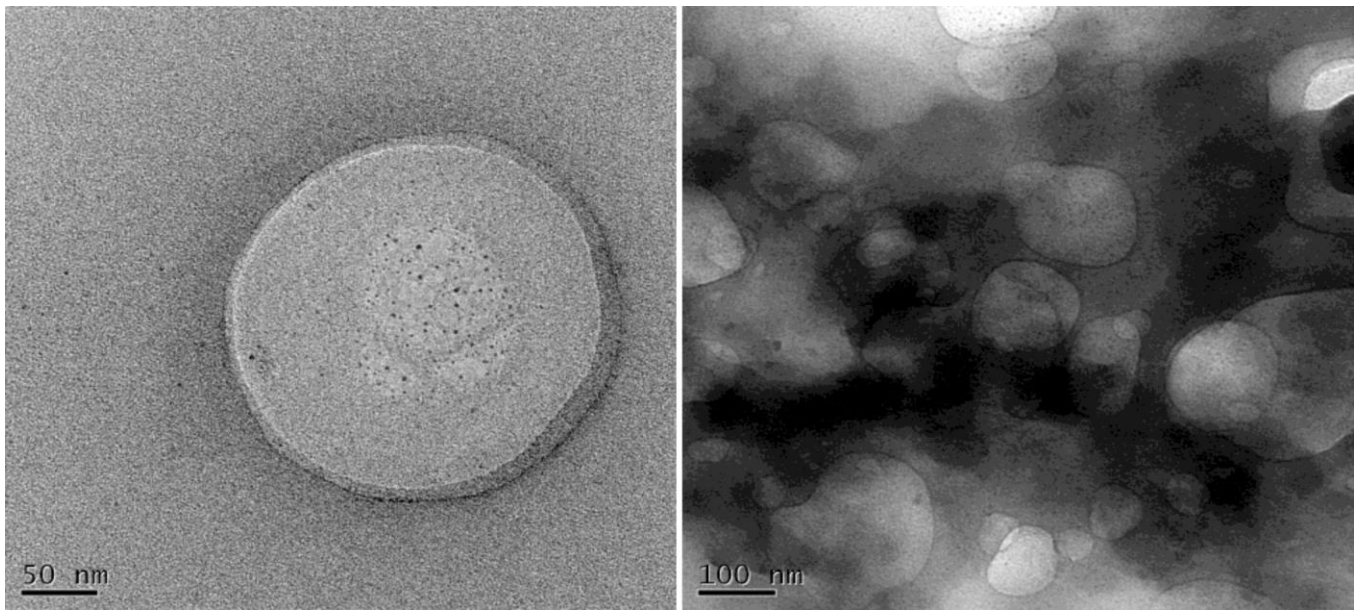

Fig. 7. HRTEM images of the nanoparticles SCCN4

FTIR study: The FTIR study was carried out for the extract and the optimized formulation (Fig. 8). The characteristic peaks at 2920 (C-H, *str.*, -CH_3), 1666 (C=O, *str.*), 1029 (-C-O-, *str.*) confirmed the presence of reported compound in the extract. In copper nanoparticles, the characteristic peaks at 2925 (C-H *str.*, -CH_3), 1104 (-C-O-, *str.*) were observed. No significant changes were observed in the absorption bands of the extract, with only minor shifts attributed to bond formation between the metal ions and extract, indicating the absence of chemical incompatibility. The formation of nanoparticles was confirmed by these shifts and changes in absorption intensity, with the appearance of a peak at 617 cm^{-1} corresponding to M–O coordination, further validating the synthesis of metallic nanoparticles. Overall, the nanoparticles formulation exhibited no chemical incompatibility.

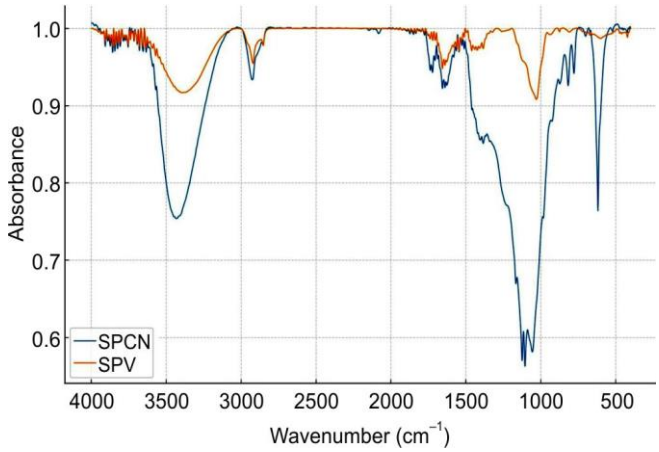

Fig. 8. Overlay FTIR spectra of extract nanoparticles SCCN4

Thermal analysis: The thermal stability of the copper nanoparticles was confirmed by TGA and DTA analyses. The TGA profile (Fig. 9a) showed a total weight loss of 3.4% from an initial 27.52 mg up to 800 ºC, with an initial 2.1% loss between 30-150 ºC attributed to moisture and adsorbed solvents, while excellent stability was observed from 200-800 ºC, indicating resistance to atmospheric decomposition and volatilization. DTA analysis (Fig. 9b) revealed an endothermic peak at 73.4 ºC corresponding to physically adsorbed moisture, a peak at 108.9 ºC due to residual solvent and surface-bound species, and a peak at 150.1 ºC associated with structural rearrangement or low-temperature crystallization, with a total area under the curve of 3399 μV/mg indicating modest transitions. No significant exothermic events or decomposition were observed, demonstrating that the optimized nanoparticles possess excellent thermal stability and a prolonged shelf life [35].

***In vitro* antioxidant activity:** The percentage inhibition was calculated and represented in Table-4. The percentage inhibition was found to be 87.52 ± 0.026 for extract, 97.27 ± 0.14 for nanoparticles and 96.41 ± 0.18 for standard at 125 μg/mL. The percentage inhibition increased in a concentration-dependent manner, with the nanoparticles exhibiting the highest activity. The IC_{50} values were determined as 109.47 μg/mL for the standard, 86.41 μg/mL for the extract and 93.72 μg/mL for the nanoparticles, indicating enhanced antioxidant potential of the extract and its nanoparticle formulation.

Anticancer activity: The *in vitro* anticancer activity was determined by MTT assay method. The data represented in Table-5 along with % cell viability. The concentration depended response was observed for extract and nanoparticles. The minimum percentage cell viability was observed at 100

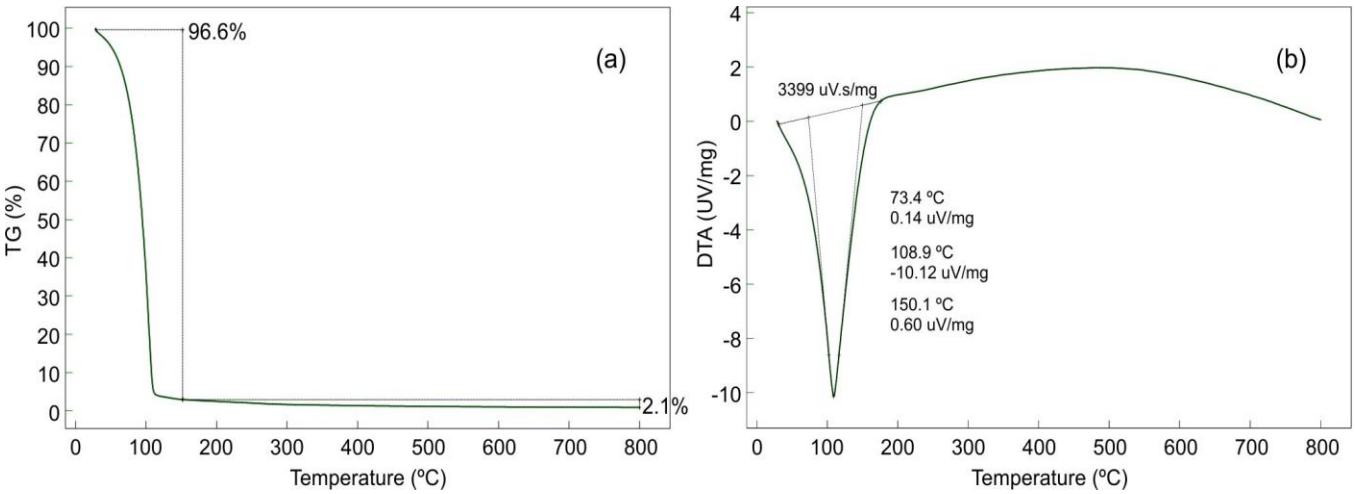

Fig. 9. (a) TGA and (b) DTA thermograms of nanoparticles SCCN4

TABLE-4
OBSERVATION FOR ANTIOXIDANT ACTIVITY IN TERMS OF DPPH METHOD

Compound No.	DPPH scavenging effect (%) [mean ± SEM]					IC_{50} (μg/mL)
	25 μg/mL	50 μg/mL	75 μg/mL	100 μg/mL	125 μg/mL	
Extract	31.25 ± 0.06	41.51 ± 0.02	53.21 ± 0.08	66.77 ± 0.15	87.52 ± 0.02	109.47
Nanoparticle	45.36 ± 0.01	58.36 ± 0.06	76.61 ± 0.05	82.35 ± 0.12	97.27 ± 0.14	86.41
Ascorbic acid	22.48 ± 0.12	41.23 ± 0.19	52.56 ± 0.20	75.42 ± 0.09	96.41 ± 0.18	93.72

All the studies carried out in triplicate and data are represented in Mean ± SEM.

TABLE-5
OBSERVATION FOR *in vitro* ANTICANCER ACTIVITY IN TERM PERCENTAGE OF CELL VIABILITY BY MTT ASSAY METHOD

Treatment	Conc. (µg/mL)	Cell line-1 (MCF7) (Mean ± SEM)	IC_{50} (µg/mL)	Cell line-2 (LNCaP) (Mean ± SEM)	IC_{50} (µg/mL)
Standard	25	78 ± 2.31	64.48	73 ± 1.732	77.54
	50	66 ± 3.46		60.33 ± 1.76	
	75	47.67 ± 2.60		44.33 ± 2.60	
	100	25.67 ± 2.33		22.67 ± 2.33	
Extract	25	96.67 ± 4.41	61.91	90.67 ± 2.72	52.67
	50	92 ± 3.21		82 ± 1.73	
	75	81 ± 2.08		58.67 ± 3.18	
	100	75 ± 5.13		31.67 ± 2.72	
Nanoparticles	25	91.33 ± 2.33	48.87	93.67 ± 2.02	48.87
	50	85.33 ± 3.18		90.67 ± 2.33	
	75	61.67 ± 2.90		83 ± 2.30	
	100	31.67 ± 2.02		71.67 ± 2.72	

All the studies carried out in triplicate and data are represented in Mean ± SEM

µg/mL. In case of MCF7 cell line the value was found to be 25.67 ± 2.33 (standard), 75 ± 5.13 (extract) and 31.67 ± 2.02 for nanoparticles. The percentage cell viability was 22.67 ± 2.33, 71.67 ± 2.72 and 31.67 ± 2.72 against LNCaP cell line. The IC_{50} value for optimized nanoparticles (48.87) was less compared to extract (61.91 & 52.67). Based on these results, it is found that the nanoparticle demonstrated higher efficacy than the extract in terms of percentage inhibition and cell viability, attributed to its reduced particle size and spherical morphology, which enhanced permeability toward the target site.

Conclusion

The chloroform extract of *Asparagus racemosus* was found to contain the steroidal compound pregn-5-ene-3,11-dione, 17,20:20,21-bis[methylenebis(oxy)]-, cyclic 3-(1,2-ethanediyl acetal) as a major constituent. *In silico* analysis indicated favourable drug-likeness and pharmacokinetic profiles, with target prediction suggesting significant anticancer activity. However, the compound and extract exhibited poor aqueous solubility, limiting their therapeutic potential. To enhance the bioavailability and efficacy, a copper nanoparticle formulation was developed and optimized using a copper salt concentration of 1 mM. The resulting copper nanoparticles displayed excellent stability, a spherical morphology with a concentric bilayer membrane and high thermal stability, indicating improved shelf life. Compared to the crude extract, the optimized copper nanoparticles demonstrated enhanced therapeutic efficacy against breast and prostate cancer, likely due to increased permeability and bioavailability.

ACKNOWLEDGEMENTS

The authors acknowledge to SAIF, IIT Bombay for GCMS, ESEM, TEM, FTIR, TGA and DTA analysis. Sincere thanks to CIF, Lovely Professional University, Phagwara, India for the particle size and zeta analysis are also acknowledged.

CONFLICT OF INTEREST

The authors declare that there is no conflict of interests regarding the publication of this article.

REFERENCES

1. M.I. Abdulazeez and M.A. Majeed, *Indian J. Med. Sci.*, **57**, 408 (2003); https://doi.org/10.1055/s-0041-1735427.
2. V. Sharma, M. Thakur, N.S. Chauhan and V.K. Dixit, *Pharm. Biol.*, **44**, 503 (2018); https://doi.org/10.1080/13880200600897556
3. T. Hongratanaworakit and G. Buchbauer, *Phytother. Res.*, **20**, 756 (2006); https://doi.org/10.1002/ptr.1950
4. G. Rameshkumar and S. Ravichandran, *Asian Pac. J. Trop. Biomed.*, **3**, 118 (2013); https://doi.org/10.1016/S2221-1691(13)60035-0
5. J. Jeevanandam, A. Barhoum, Y.S. Chan, A. Dufresne and M.K. Danquah, *Beilstein J. Nanotechnol.*, **9**, 1050 (2018); https://doi.org/10.3762/bjnano.9.98
6. S. Sangeetha, N. Geetha and R. Kumar, *Mater. Lett.*, **282**, 128794 (2021); https://doi.org/10.1016/j.matlet.2020.128794
7. L.F. Hussein, F.S. Abbas, A. Al-Balhawi, A.S.D. AL-Ridha and H.H. Hussein, *Mater. Today Proc.*, **56**, 2714 (2022); https://doi.org/10.1016/j.matpr.2021.09.396
8. Y. Kohl, M. Hesler, R. Drexel, L. Kovar, S. Dähnhardt-Pfeiffer, D. Selzer, S. Wagner, T. Lehr, H. von Briesen and F. Meier, *Nanomaterials*, **11**, 1358 (2021); https://doi.org/10.3390/nano11061358
9. J.L. Axson, D.I. Stark, A.L. Bondy, S.S. Capracotta, A.D. Maynard, M.A. Philbert, I.L. Bergin and A.P. Ault, *J. Phys. Chem. C*, **119**, 20632 (2015); https://doi.org/10.1021/acs.jpcc.5b03634
10. G. Sharma, A.R. Sharma, J.S. Nam, G.P.C. Doss, S.-S. Lee and C. Chakraborty, *J. Nanobiotechnol.*, **13**, 74 (2015); https://doi.org/10.1186/s12951-015-0136-y
11. S. Iravani, *Green Chem.*, **13**, 2638 (2011); https://doi.org/10.1039/c1gc15386b
12. R. Rajan, V. Duraipandiyan and S. Ignacimuthu, *J. Nanosci. Nanotechnol.*, **20**, 120 (2020); https://doi.org/10.1166/jnn.2020.17040
13. P. Singh, S. Pandit, V.R.S.S. Mokkapati, V.A. Garg, V. Ravikumar and I. Mijakovic, *Int. J. Mol. Sci.*, **19**, 1979 (2018); https://doi.org/10.3390/ijms19071979
14. M. S. Usman, M. E. E. Zowalaty, K. Shameli, N. Zainuddin, M. Salama, N.A. Ibrahim, *Int. J. Nanomedicine*, **8**, 4467 (2013); https://doi.org/10.2147/IJN. S50837
15. S.H. Rasheed, R.K. Vakkalagadda, S. Mustak and S. Sen, *Pharmacogn. Res.*, **16**, 161 (2023); https://doi.org/10.5530/pres.16.1.21
16. N. Chaudhary, M.B. Siddiqui and S. Khatoon, *Indian J. Tradit. Knowl.*, **13**, 543 (2014).
17. S.H. Rasheed, S. Mustak, C. Mohanty, R.K. Vakkalagadda and S. Sen, *Asian J. Chem.*, **36**, 1903 (2024); https://doi.org/10.14233/ajchem.2024.31671

18. S. Sen, B. Roy, N. Kannappan, K. Zoghebi, M. Albratty, H.A. Alhazmi, A. Najmi and M.S. Alam, *Pharmacogn. Mag.*, **21**, 1100 (2025); https://doi.org/10.1177/09731296241300873
19. S. Sen, K. Swathi, D. Vishwanath, B. Ravindar, M. Chaitanya, S. Tejasree, S. Cherukupally and H.V. Santhoshi Allu, *Pharmacognosy Res.*, **16**, 887 (2024); https://doi.org/10.5530/pres.16.4.101
20. S. Lal, K. Prakash, S. Hooda, V. Kumar and P. Kumar, *J. Mol. Struct.*, **1200**, 127003 (2020); https://doi.org/10.1016/j.molstruc.2019.127003
21. S. Sen, B. Ravindar, S. Jala, L. Dharabonia and K. Rajeshwari, *Res. J. Pharm. Technol.*, **16**, 2239 (2023); https://doi.org/10.52711/0974-360X.2023.00368
22. W. Maryana, A. Rahma, D. Mudhakir and H. Rachmawati, *J. Biomimet. Biomater. Biomed. Eng.*, **25**, 54 (2015); https://doi.org/10.4028/www.scientific.net/JBBBE.25.54
23. S. Kumar, K. Deivasigamani and B. Roy, *Pharmacogn. Mag.*, **19**, 371 (2023); https://doi.org/10.1177/09731296231157192
24. M. Kumar, D. Himaja and S. Sen, *Indian J. Chem.*, **59A**, 1120 (2020).
25. O. Mahapatra, M. Bhagat, C. Gopalakrishnan and K.D. Arunachalam, *Biol. Trace Elem. Res.*, **197**, 29 (2020); https://doi.org/10.1007/s12011-019-01919-2
26. S. Sen, B. De and T.S. Easwari, *Asian J. Chem.*, **26**, 6616 (2014); https://doi.org/10.14233/ajchem.2014.17003
27. F. Tavares-Carreón, S. De la Torre-Zavala, H.F. Arocha-Garza, V. Souza, L.J. Galán-Wong and H. Avilés-Arnaut, *PeerJ*, **8**, e8686 (2020); https://doi.org/10.7717/peerj.8686
28. B.O. Sadia, J.K. Cherutoi and C.M. Achisa, *J. Nanotechnol.*, **561**, 1434 (2021); https://doi.org/10.1155/2021/5611434
29. M. Pourmadadi, R. Holghoomi, A. Shamsabadipour, R. Maleki-baladi, A. Rahdar and S. Pandey, *Plant Nano Biol.*, **8**, 100070 (2024); https://doi.org/10.1016/j.plana.2024.100070
30. S. Shaker, A.R. Gardouh and M.M. Ghorab, *Res. Pharm. Sci.*, **12**, 346 (2017); https://doi.org/10.4103/1735-5362.213979
31. G.P. Kumar and P. Rajeshwarrao, *Acta Pharm. Sin. B*, **1**, 208 (2011); https://doi.org/10.1016/j.apsb.2011.09.002
32. H. Refai, D. Hassan and R. Abdelmonem, *Drug Deliv.*, **24**, 278 (2017); https://doi.org/10.1080/10717544.2016.1247925
33. R. Umamaheswari and S. Kothai, *Res. J. Pharm. Technol.*, **13**, 4357 (2020); https://doi.org/10.5958/0974-360X.2020.00770.2
34. A. Haeri, B. Alinaghian, M. Daeihamed and S. Dadashzadeh, *Iran J Pharm. Res.*, **13**(**Suppl**), 3 (2014).
35. J.M. Rami, C.D. Patel, C.M. Patel and M.V. Patel, *Mater. Today Proc.*, **43**, 655 (2021); https://doi.org/10.1016/j.matpr.2020.12.554